Author Manuscript

Author Manuscript

Author Manuscript

Author Manuscript

HHS Public Access

Author manuscript

Am J Med Genet A. Author manuscript; available in PMC 2015 March 04.

Published in final edited form as:

Am J Med Genet A. 2014 January ; 0(1): 17–28. doi:10.1002/ajmg.a.36189.

A Novel Germline PIGA Mutation in Ferro-Cerebro-Cutaneous Syndrome: A Neurodegenerative X-Linked Epileptic Encephalopathy With Systemic Iron-Overload

Kathryn J. Swoboda[1,*], **Rebecca L. Margraf**[2,*], **John C. Carey**[3,4], **Holly Zhou**[5], **Tara M. Newcomb**[1], **Emily Coonrod**[2], **Jacob Durtschi**[2], **Kalyan Mallempati**[2], **Attila Kumanovics**[2,5], **Ben E. Katz**[7], **Karl V. Voelkerding**[2,5], and **John M. Opitz**[3,4,5,6]

[1]Pediatric Motor Disorders Research Program, Department of Neurology, University of Utah School of Medicine, Salt Lake City, Utah

[2]ARUP Institute for Clinical and Experimental Pathology®, ARUP Laboratories, Salt Lake City, Utah

[3]Department of Obstetrics and Gynecology, University of Utah School of Medicine, Salt Lake City, Utah

[4]Department of Pediatrics, Division of Medical Genetics, University of Utah School of Medicine, Salt Lake City, Utah

[5]Department of Pathology, University of Utah School of Medicine, Salt Lake City, Utah

[6]Department of Human Genetics, University of Utah School of Medicine, Salt Lake City, Utah

[7]Private Practice of Pediatrics and Pediatric Neurology, Twin Falls, Idaho

Abstract

Three related males presented with a newly recognized x-linked syndrome associated with neurodegeneration, cutaneous abnormalities, and systemic iron overload. Linkage studies demonstrated that they shared a haplotype on Xp21.3– Xp22.2 and exome sequencing was used to identify candidate variants. Of the segregating variants, only a *PIGA* mutation segregated with disease in the family. The c.328_330delCCT *PIGA* variant predicts, p.Leu 110 del (or c. 1030_1032delCTT, p. Leu344del depending on the reference sequence). The unaffected great-grandfather shared his X allele with the proband but he did not have the *PIGA* mutation, indicating that the mutation arose de novo in his daughter. A single family with a germline *PIGA* mutation has been reported; affected males had a phenotype characterized by multiple congenital anomalies

© 2013 Wiley Periodicals, Inc.

*Correspondence to: Kathryn J. Swoboda, M.D., F.A.C.M.G., Pediatric Motor Disorders Research Program, Department of Neurology, University of Utah School of, Medicine, 30 North, 1900 East, 3R149, Salt Lake City, UT 84132. swoboda@genetics.utah.edu.

Kathryn J. Swoboda and Rebecca L. Margraf contributed jointly to critical aspects of this work.

Conflict of interest: KJS has received grant funding from the National Institutes of Child Health and Disease, the National Institutes of Neurologic Disease and Stroke, the Muscular Dystrophy Association and the Alternating Hemiplegia of Childhood Foundation. She has clinical trial contracts with ISIS Pharmaceuticals and Biomarin. She has served as a paid consultant to Novartis and BioLife Stem Cell. The other authors have no conflict of interest to report.

Web Resources: Online Mendelian Inheritance in Man (OMIM), http://www.omim.org/

Author Manuscript Author Manuscript Author Manuscript Author Manuscript

and severe neurologic impairment resulting in infantile lethality. In contrast, affected boys in the family described here were born without anomalies and were neurologically normal prior to onset of seizures after 6 months of age, with two surviving to the second decade. *PIGA* encodes an enzyme in the GPI anchor biosynthesis pathway. An affected individual in the family studied here was deficient in GPI anchor proteins on granulocytes but not erythrocytes. In conclusion, the PIGA mutation in this family likely causes a reduction in GPI anchor protein cell surface expression in various cell types, resulting in the observed pleiotropic phenotype involving central nervous system, skin, and iron metabolism.

Keywords

iron; Ferro-Cerebro-Cutaneous syndrome; exome; sequencing; *PIGA*; PIG-A protein; epilepsy; encephalopathy; hemochromatosis; microcephaly; cerebellar atrophy; seizures; neurodegeneration; X-linked; recessive

INTRODUCTION

Iron storage disorders are categorized into those with systemic iron deposition and those with primary central nervous system iron accumulation. Primary or hereditary hemochromatosis, the most common systemic iron storage disorder, is an autosomal recessive adult-onset disease caused by mutations in *HFE*, resulting in a range of symptoms including arthritis, diabetes, hypothyroidism, heart abnormalities, liver disease, and cutaneous hyper pigmentation. Disorders associated with primary systemic iron deposition in infants include the perinatal and neonatal hemochromatoses (neonatal iron storage disease or NISD). Gestational alloimmune factors resulting in abnormal fetoplacental iron handling and intrauterine liver damage are thought to contribute to pathogenesis in most affected infants, although autosomal recessive inheritance has been suggested in some cases [Collardeau-Frachon et al., 2012]. Excess hepatic iron is also present in peroxisomal disorders such as Zellweger syndrome, although the pathogenesis and clinical presentation are typically distinct from NISD. Primary recessive hemochromatoses with childhood onset are rare, and occur in association with mutations in the genes hemojuvelin (*HJV*), hepcidin (*HAMP*), transferrin receptor 2 (*TRF2*), and ferroportin (*SLC40A1*). None of the primary systemic hemochromatoses reported to date are associated with neurodegeneration [Santos et al., 2012]. Neurodegeneration with brain iron accumulation (NBIA) is a heterogeneous group of disorders associated with iron deposition most prominently in basal ganglia and is distinct from the systemic iron storage disorders.

We describe a three-generation family with three affected boys with a progressive neurodegenerative condition characterized by an infantile-onset epilepsy and encephalopathy in association with systemic iron overload. Here, we present the clinical, molecular, and functional characterization of this disorder.

Author Manuscript Author Manuscript Author Manuscript Author Manuscript

PATIENTS AND METHODS

Patients

The University of Utah Institutional Review Board approved this study. DNA extraction from peripheral blood samples was performed by the genomic core facility at the University of Utah Clinical Center for Translational Science. Extracted DNA from four family members was submitted for exome sequencing: affected individuals IV-3 and III-9, unaffected female III-2, and unaffected male IV-4 (Fig. 1). A DNA sample from individual III-9 was derived from a transformed lymphoblast cell line; for the rest, DNA was extracted directly from peripheral blood samples. Samples of DNA from several additional family members were used for Sanger sequencing to verify variants detected by exome sequencing (Fig. 2).

Laboratory Studies

Peripheral blood samples for iron studies, cell counts, and cell surface marker measurements via flow cytometry and biochemical measurements were performed at ARUP laboratories, University of Utah, per routine clinical assays.

Exome Sequencing

For each family member, 2.5 μg of intact genomic DNA was fragmented to a 300–400 bp size distribution using adaptive focused acoustics (Covaris, Inc., Woburn, MA). Fragments were converted to libraries by end-repair and ligation with specific adapters using an automated instrument (SPRI-TE Nucleic acid extractor, Beckman Coulter Genomics, Danvers, MA). Adapter-ligated fragment libraries were amplified in eight PCR reactions (50 μl each) using paired end PCR primers 1.0 and 2.0, then combined and passed over a column with a 50 μl elution volume (Qiaquick, Qiagen Corp, Gaithersburg, MD). Exome-in-solution capture was performed (SeqCap EZ Human Exome Library v2.0 reagents, Roche Nimblegen, Madison, WI) according to the manufacturer's instructions. Following the post-capture PCR step, libraries were gel-purified in the 475 ± 50 bp range. Library steps were checked for fragment size and DNA concentration (Bioanalyzer 2100, Agilent Technologies, Inc., Santa Clara, CA). Library concentrations were determined using qPCR (KAPA Library Quant Kit, Kapa Biosystems, Inc., Woburn, MA). The libraries were denatured, diluted to 7pM and introduced into the Illumina cBot instrument for cluster generation, followed by sequencing on the HiSeq 2000 instrument with 100 base length pair end reads using version 2 chemistry (Illumina protocol part# 15012045 RevC April 2010, and part# 15019437 RevB October 2010).

Sequence Alignment and Variant Calling

Each of the four samples was exome sequenced using one lane of a flow cell v2 resulting in an average of 410,000 clusters/mm^2 (while the target was 450 clusters/mm^2) and an average 95.8% of the clusters passing the HiSeq sequencing software filter. An average of 9.4 Gb of 100 base, paired-end reads were generated per sample.

Illumina HiSeq 2000 FastQ files were aligned to the human reference genome (GRCh37.1) using BWA (BWA version 0.6.1, http://bio-bwa.sourceforge.net/) with default parameters.

Author Manuscript Author Manuscript Author Manuscript Author Manuscript

Average coverage of targeted exome regions was 112. The alignments were refined using GATK (GATK version 1.6–11, http://www.broad-institute.org/gatk/) for local realignment around indels, followed by duplicate removal (Sam tools version 0.1.18, http://samtools.sourceforge.net/, and then followed by GATK base quality score recalibration [DePristo et al., 2011]. Variant calls from the alignment data used the GATK Unified Genotyper. Variants with a variant quality score less than 30 were not included in any further analysis. Variants were additionally filtered using the GATK best practices hard filters that included (for SNVs): QD<2.0, MQ < 40.0, FS > 60.0, HaplotypeScore > 13.0, MQ Rank Sum < −12.5, and Read Pos Rank Sum < −8.0. Hard filters for Indels included QD < 2.0, Read Pos Rank Sum < −20.0, or FS > 200.0. Final variant lists were formatted in vcf file format.

Candidate Gene Identification

The variant file (.vcf) for each sample was imported into Golden Helix SVS software (version 7.6.8, Golden Helix, Inc., Bozeman, MT) for filtering and intersecting variants between family members. Variants included in the analysis were those with >3 read coverage over the variant position, localized to exons ±10 bases, and with <5% MAF (minor allele frequency) [The 1000 Genomes Project Consortium, 2010]. The X chromosome variants that were hemizygous in the unaffected brother IV-4 or homozygous in the unaffected mother III-2 were eliminated from the variant pool identified by intersection of the X chromosome hemizygous changes in the two affected males (IV-3 and III-9). To analyze for X-linked inheritance specifically, the remaining hemizygous variants then were intersected with maternal X chromosome heterozygous variants. The X chromosome candidate genes from the suspected disease gene linkage interval were also evaluated manually by using iGV software (The Integrative Genomics Viewer, Broad Institute) and the bam files (read alignment data).

CLINICAL REPORTS

Patient III-9

The propositus (III-9) was the seventh child born to a then 35-year-old mother; pregnancy, labor, delivery, and early infancy were normal. His birth weight was 3,681 g. His first seizure occurred at age 7 months during a febrile illness. At 9 months of age, the earliest documented head circumference was 44 cm (10th–25th centile). By 17 months, he had had multiple episodes of status epilepticus. An EEG demonstrated generalized background slowing and predominantly posterior bursts of sharp, slow and spike wave activity. Head growth had decelerated (OFC 46 cm, 10th centile). By *3*½ years, he had a coarse face, alveolar ridge overgrowth, and tapered fingers. He was non-ambulatory, nonverbal and in a largely “vegetative” state, with roving eye movements, axial hypotonia, increased lower extremity tone, brisk reflexes and bilateral grasp, and Babinski responses; he continued to manifest frequent intermittent seizures. By 4½ years of age, he was cortically blind and deaf, had microcephaly (OFC 46.5 cm, <3rd centile), and demonstrated intermittent stimulus-sensitive myoclonus. A firm liver edge extended ∼7–8 cm below the right costal margin. He died of aspiration pneumonia at almost 7 years of age.

Author Manuscript Author Manuscript Author Manuscript Author Manuscript

Electron microscope leukocyte studies performed on individual II-9 at age 17 months showed lymphocytes with small myelin figures and clusters of vacuoles with electron dense tubules; a siderosome was noted in retrospect (Fig. 3).

At autopsy, individual III-9 had atrophic and contracted limbs; the lungs were diffusely consolidated; the abdomen was protuberant with a gastrostomy site and evident hepatosplenomegaly (liver weight 968 g). Liver sections showed uniform red–brown parenchyma; no microscopy was performed. The brain weight was 960 g, significantly diminished for age, with generalized cortical and cerebellar atrophy. Electron micrographic studies of frontal cortex showed membrane-bound fibrillar reticular inclusions in several neurons, astrocytes and presumed mesenchymal cells associated with blood vessels and disorganized mitochondria (Fig. 4).

Patient III-10

Patient III-10 was the eighth child born to his now 39-year-old mother. He was delivered following a term uncomplicated pregnancy, with normal growth parameters, birth weight 2,407 g. By 6 months, he manifested abnormal eye movements with head bobbing. Seizures began at 7 months, head circumference was 44.6 cm (50th centile) and his height was 68 cm (50th centile). By 14 months he had lost head control and was encephalopathic; by 18 months he had severe generalized spasticity and plagiocephaly with head circumference of 46.8 cm (25th–50th centile). He had a firm liver edge, palpable several centimeters below the right costal margin. He had microdontia, with widely spaced teeth and delayed eruption; several were absent. By 2½ years, he had microcephaly, recurrent status epilepticus and was non-verbal, with severe cortical visual impairment and a nearly continuous postural tremor. His head circumference was 47.8 cm at 2½ years (<2nd centile). Figure 5 shows patient III-10 as an infant, 3a and several years later, 3b. By 10 years of age, he had striking hepatomegaly and splenomegaly. At 12 years of age, he experienced an episode of thrombocytopenia, which was responsive to corticosteroid administration but not to withdrawal of valproic acid. He developed generalized flexion contractures, foot deformity, and muscle atrophy. His condition progressively worsened and he died of liver failure at almost 16 years of age.

Notable laboratory finding included twice normal CSF glutamate levels (906, nl 150–550), as well as other abnormalities consistent with terminal liver failure; however, excess iron storage was not suspected prior to autopsy and serum iron studies were not performed.

External exam showed truncal obesity, small stature for age (15 years), scoliosis, generalized joint contractures, and a gastrostomy tube. He had obvious ascites with marked splenomegaly and macro and micronodular cirrhosis, with extensive iron deposition in liver, kidney, pancreas, and gastrointestinal epithelium adrenal glands (Fig. 6). Lung changes consistent with chronic and acute aspiration pneumonia, myocardial hypertrophy of the left ventricle, multiple brownish skin papules consistent with psoriasis, mild scoliosis, and atrophic testes were also present.

Brain weight was half of that expected for age (884 g); grossly, the right temporal lobe, both occipital lobes and the cerebellum were markedly atrophic. The meninges were thickened

Author Manuscript Author Manuscript Author Manuscript Author Manuscript

and darkly pigmented, but vessels and optic nerves appeared normal. There was moderate dilatation of the ventricular system. The pons, midbrain, and medulla appeared normal. Microscopic sections demonstrated marked thinning of the cerebral cortex with neuronal loss and longstanding gliosis; in some areas, there was more severe gliosis with spongy changes in the cortical neuropil and relative neuronal sparing. Sections of the left frontal lobe did not show neuronal loss or gliosis, although there were scattered Alzheimer type 2 astrocytes. In contrast, the right and left occipital lobes demonstrated marked cortical thinning and gliosis with scattered intact neurons. Other portions of the cortex showed no neuronal loss or gliosis. White matter adjacent to the gliotic cortex demonstrated loss of tracts and gliosis. The sections of "damaged" cortex showed scattered ferruginated neurons, typical of the pattern seen with ischemic anoxia. The cerebral peduncles demonstrated lateral pallor. The sub-stantia nigra neurons were small, but the melanin pigment was present and Prussian blue stain did not show excess iron. The medulla demonstrated loss of neurons in the inferior olive with gliosis. The cerebellum demonstrated severe Purkinje cell loss with Bergmann gliosis and thinning of the molecular and the granular cell layers. Neurons in the dentate and caudate nuclei showed scant hemosiderin in droplets in rare cells, but the neuronal population was normal and there was no evident gliosis. The iron stain also demonstrated only scant iron-positive material. The insular cortex demonstrated loss of neurons and gliosis. The pathologist noted that the focal severe loss of cortical neurons in the right temporal lobe and the occipital lobes was considered unusual of typical anoxic damage, and the sparing of some neurons within this severely cystic gliotic area of the cortex was more suggestive of a metabolic disorder. A mitochondrial abnormality was considered since the cystic areas in the cortex with scattered normal neurons were reminiscent, although distinct, from the microscopic lesions seen in Leigh disease due to lack of vascular proliferation. The deposition of iron in the basal ganglia was considered scant, and would not be uncommon in an older person, but considered possibly significant in light of the age of the subject (Fig. 7).

Patient IV-3

Patient IV-3 was the nephew of the two brothers described above and was the third child born to a 26-year-old mother. Pregnancy, delivery, and early infancy were unremarkable. Birth weight was 4,530 g, length was 39.4 cm and OFC was 39.4 cm (>98th centile). By 6 months of age, he was hypotonic and ataxic and he began manifesting intermittent eye movement abnormalities. At 9 months of age, he had his first clinical seizure and his psychomotor development decelerated. He demonstrated brachycephaly, delayed eruption of teeth, and an anteriorly tethered tongue. He was unable to sit, and demonstrated truncal ataxia, episodic seizure activity, and eye movement abnormalities and oromotor dystonia. By the age of 5½ years, he had regressed considerably, and his head growth had decelerated to the 50th centile (53 cm); he had encephalopathy, refractory epilepsy, generalized muscular atrophy, spasticity, extensor plantar responses, and limb contractures. He had hepatomegaly but no jaundice or splenomegaly. He required a gastrostomy tube for feeding. In subsequent years, he developed progressive hepatosplenomegaly and serum iron studies indicated increasing systemic iron overload. At age 15 years, he was profoundly encephalopathic, cortically blind, and deaf, with permanent limb contractures, and frequent

Author Manuscript Author Manuscript Author Manuscript Author Manuscript

seizures with head circumference of 54 cm (25th–50th centile). Figure 5 shows patient IV-3 as an infant, 3c, and as a teenager, 3d.

Notable laboratory findings included evidence of systemic iron overload at 5½ years of age with elevated hemoglobin (15.1 g/dl, normal 11.5–13.5 g/dl) and hematocrit levels (43.4%, normal 34.0– 40.0%); increased total serum iron (227 μg/day, normal 50–120); elevated iron saturation (79%, normal 20–50); and elevated serum ferritin (485 ng/ml, normal 7–140). A liver biopsy showed mild lobular disarray, minimal steatosis, granular pigmentation of hepatocytes predominantly in zone I, grade II/IV iron storage, and mild triaditis but no cirrhosis.

Features and Findings in Common to All Three Patients

In addition to their neurologic manifestations, the patients had ichthyosis or seborrheic dermatitis to varying degrees, with dryness and desquamation of plaque-like brownish scales most pronounced in the axillae and extending to the upper back, neck, and ears in a streak-like manner (Fig. 8). Other cutaneous features included epidermal microabscesses involving the trunk and scalp, and circular lesions on palms and soles (Fig. 9a and c). Oral abnormalities included microdontia, widely spaced, and pointed teeth, and gingival overgrowth (Fig. 9b). Cranial imaging in all three boys was initially normal (CT scans for patient III-9 at the age of 7 and 10 months, patient III-10 at 7 months, and both CT and MRI were normal at 7 and 8 months for patient IV-3). Cranial MRI imaging subsequently demonstrated progressive ventricular dilatation with generalized cortical and especially cerebellar atrophy and white matter loss by the age of (5.5 years, 11 years, and 3 years 9 months, respectively). Figure 10 shows this progression for individual IV-3 with serial MRI imaging.

RESULTS

Karyotype with GTG banding was normal in patients III-9 and III-9. Fragile X studies were normal in all three patients. High Resolution Karyotype and Telomeric FISH studies were normal in patient IV-3. Linkage studies demonstrated a shared haplotype in affected boys and their carrier mothers at Xp21.3–22.2, with critical flanking recombinants at DXS1189 (hg19 ChrX: 11,597,674–11,798,674) and DXS8039 (hg19 ChrX: 30,118,267–30,318,613), encompassing an 18-megabase region containing more than 100 genes. We performed Sanger sequencing of several candidate genes within this region; however, these efforts proved unsuccessful in identifying a disease-causing variant (data not shown). Given the overlapping phenotype in this family with that reported with DNA Polymerase Gamma I (*POLG1*) mutations, clinical diagnostic testing was performed. Sequencing identified a heterozygous missense mutation in *POLG1* in IV-3, c.1402A>G (p.Asn468Asp), of uncertain significance. Although this missense mutation had been reported in patients with mitochondrial phenotypes, SIFT and PolyPhen algorithms predict a benign change; further, this change was heterozygous in carrier patient III-2, hemizygous in an unaffected male, patient IV-4, and absent in affected patient III-10 [Luoma et al., 2004; González-Vioque et al., 2006]. We conclude from these data that this variant did not contribute to the phenotype in the three boys described here, primarily on the basis of the segregation data.

Author Manuscript Author Manuscript Author Manuscript Author Manuscript

Exome Sequencing and Variant Discovery

Exome sequencing data were generated from four family members; two were affected (IV-3 and III-9) and two were unaffected (III-2 and IV-4). A heuristic variant filtering approach resulted in four X-linked candidate genes within the linkage region: *PDHA1* (intronic variant, g.19367346C>T), *PTCHD1* (missense variant, g.23410745C>G), *PIGA* (inframe 3 bp deletion, g.15342943–15342945delAAG), and *PHKA2* (missense variant rs17313249, g. 18972497 C>G). These gene variants were also found by reviewing likely causative genes within the X chromosome linkage region using iGV to view the exome data. None of these variants was found in 1,000 genomes or 5400 exome data and they all followed the expected inheritance patterned in dicating that all four variants were linked to the same allele. The *PIGA* and *PDHA1* variants were not found in the 1,000 genomes or NHLBI Exome Sequencing Project 6503 exome data [The 1000 Genomes Project Consortium, 2010], so they are novel, while the *PTCHD1* change is rare (0.02% population frequency). *PHKA2* was eliminated from further analysis, since the variant was too common (1.6–3.6% frequency) to cause this rare disorder.

Two other X chromosome genes in the linkage region with uncommon variants, *ZRSR2* (g. 15838411C>T, within 500,000 bases of the *PIGA* gene variant) and *PRPS2* (g. 12817576C>A), were also chosen for analysis. DNA from the extended family was Sanger sequenced for five linked variants (in genes *PTCHD1*, *PDHA1*, *ZRSR2*, *PIGA*, and *PRPS2*) within the X chromosome linkage interval region to determine segregation in the family (Fig. 1). The X chromosome origin was traced to the individual I-1, and his X chromosome contained all the linked variants except for the *PIGA* deletion and he was unaffected by the disease of the propositus. The other rare variants associated with potential candidate genes (*PTCHD1* and *PDHA1*) in the linkage interval region were present in the individual I-1, eliminating them as candidates. The *PIGA* deletion was present only in affected individuals and was not present in unaffected individuals, including the great-grandfather. Family members III-2 and III-6 were heterozygous for the *PIGA* deletion variant and were carriers of the variant. Family members IV-2 and IV-6 did inherit the X chromosome that originally harbored the *PIGA* variant, but had a recombination crossover before the *PIGA* gene, eliminating the mutation from their genomes. We conclude that the most likely model for the genetic data in this family is that the *PIGA* deletion arose as a de novo mutation transmitted by individual I-1 to individual II-2 (DNA not available), who then passed the *PIGA* mutation to several offspring.

The Sanger sequencing of genomic DNA confirmed that the *PIGA* gene had a 3-bp in frame deletion (deleted positions chrX: 15342943–15342945) in the affected individuals IV-3 and III-9 (hemizygous deletion) and was heterozygous in the females III-2 and III-6 (Fig. 2a). This *PIGA* variant is in exon 4 (c.328_330delCTT, p.Leu110del) or exon 5 (c. 1030_1032delCTT, p.Leu344del) depending on the reference sequence, NM_020473.3 or NM_002641.3, respectively. The leucine residue that is deleted in the patients is conserved from humans to zebrafish and fruit fly (Fig. 2b), and a change from leucine to any other amino acid at this position is predicted to be deleterious by SIFT.

Author Manuscript Author Manuscript Author Manuscript Author Manuscript

Flow Cytometry and FLAER Studies

To further evaluate if the *PIGA* deletion variant affected glycosyl-phosphatidylinositol (GPI) anchor biosynthesis, flow cytometry was performed. The GPI-anchored proteins CD59, CD14, and CD24 were assayed on several blood cell types in individual IV-3, and was supplemented with analysis of the FLAER stain for total GPI expression(Fig. 11). Red blood cell CD 59 levels were equivalent to normal controls (average of 10 normal samples). Although monocyte numbers were reduced in this patient, cell surface GPI expression (CD14 and FLAER stain) were in the range of the control values. In contrast, the patient's granulocyte numbers were slightly increased and both the FLAER stain and CD24 cell surface levels were reduced compared to the normal controls (Fig. 11).

DISCUSSION

The syndrome we describe here appears to represent a previously undescribed neurodegenerative disorder restricted to males, with associated systemic iron storage and distinctive cutaneous abnormalities that became apparent only after the onset of neurologic symptoms. We suggest that this disorder be designated as the Ferro-Cerebro-Cutaneous syndrome. Exome sequencing data identified a mutation in *PIGA* in a family with this disorder. Exome sequencing was used to identify candidate genes within the previously identified linkage region and also to analyze for non-linkage region candidates associated with iron homeostasis and regulation. The germline *PIGA* mutation detected was a 3-bp in-frame deletion that predicts the loss of one codon from the PIGA protein, p. Leu110del. This mutation likely arose de novo during meiosis in individual I-1 and was transmitted to II-2, since I-1 has the same X chromosome haplotype as his affected descendants lacking only the *PIGA* deletion mutation (Fig. 1). Individual II-2's DNA was not available for study, but she had several children with the X chromosome harboring the *PIGA* deletion mutation, confirming that she was an obligate carrier.

GPI anchor pathway, which adds a phosphatidylinositol glycan (PIG) class A moiety onto proteins in the endoplasmic reticulum, is composed of more than 20 PIG family genes [Kinoshita et al., 1997, 2008]. The PIGA enzyme, along with five other PIG proteins, adds N-acetylglucosamine to free phosphatidylinositol, the initiating step of the GPI anchor biosynthesis pathway. Additional PIG enzymes are important in generating the mature GPI anchor structure (e.g., PIGM and PIGV have a role in adding mannose and PIGN has a role in ethanolamine phosphate additions). The GPI anchor proteins are destined to reside on the cell surface and use the GPI moiety to anchor into the plasma membrane. It is known that a loss of, or reduced activity of, PIGA results in absent or reduced GPI-anchored proteins found on cell surfaces. A well-known example of GPI deficiency occurs in the acquired hematologic disease paroxysmal nocturnal hemoglobinuria (PNH [MIM 300818]) [Ware et al., 1994]. In PNH, somatic mutations of *PIGA* in hematopoietic stem cells leads to decreased expression of GPI-anchored proteins on the surfaces of red blood cells, B cells, and granulocytes. In particular, reduced expression of the GPI-anchored protein CD59 on red blood cells makes them susceptible to complement mediated cell lysis resulting in hemoglobinuria.

Author Manuscript Author Manuscript Author Manuscript Author Manuscript

Historically, germline *PIGA* mutations were presumed to be lethal in humans, since conventional knockout of *Piga* in mice with low levels of chimerism showed a high rate of embryonic lethality. Female mice mosaic for *Piga* null status demonstrated somatic cell selection in critical tissues, with predominantly wild-type activity in heart, liver, lung, brain, and kidney, suggesting a critical role for GPI linked proteins in these tissues [Keller et al., 1999]. In contrast, relatively equal expression of cells expressing the wild-type or recombinant allele were noted in spleen, thymus, and red cells. These mosaic mice demonstrated orofacial developmental anomalies resulting in suckling difficulties precluding their survival. Johnston et al. [2012], described the first inherited germline mutation in *PIGA* in three male infants with multiple congenital anomalies including craniofacial anomalies, congenital joint contractures, atrial septal defect, and a duplicated renal collection system, a disorder now designated multiple congenital anomalies, hypotonia and seizures type 2, MCAHS2 (MIM 300868). Affected males had significant brain anomalies including congenital macrocephaly, thin corpus callosum, prominent sulci and ventricles, white matter abnormalities, and cerebellar hypoplasia evident on neuroimaging studies; autopsy of one infant further demonstrated absent olfactory bulbs and tracts, a simplified inferior olive and a dysplastic basis points. Affected infants manifested severe neurologic impairment from birth, including hypotonia, congenital joint contractures, neonatal encephalopathy, and myoclonic epilepsy with burst-suppression on electroencephalogram; all died in early infancy [Johnston et al., 2012]. The mutation in this family introduced a stop codon in the 3-prime end of the gene, resulting in a prematurely truncated protein. Diminished GPI activity due to this mutation was demonstrated in an in vitro cellular assay, evidence that the role of PIGA in GPI anchor biosynthesis is critical for normal central nervous system development [Johnston et al., 2012].

Germline mutations in several other genes affecting the GPI anchor biosynthesis pathway cause syndromes encompassing an increasingly broad range of phenotype with widely variable neurologic involvement, including a new subclass of congenital disorders of glycosylation [Jaeken, 2011]. These genes include *PIGL* (OMIM 605947), *PIGM* (OMIM 610723), *PIGN* (OMIM 606097), *PIGO* (OMIM614730), *PIGV* (OMIM 610274), and *PGAP2*, a gene critical for correct processing and stable expression of GPI-an-chored proteins; autosomal inheritance is recessive in all cases reported to date. Mutations in *PIGL* have been reported in patients with CHIME syndrome, also known as Zunich neuroectodermal syndrome (OMIM 280000); phenotypic features include coloboma, congenital heart disease, ichthyosiform dermatosis, intellectual disability, and ear anomalies [Ng et al., 2012]. A mutation in *PIGM* was reported in a single patient with absence epilepsy and portal venous thrombosis [Almeida et al., 2006]. Mutations in *PIGN* result in multiple congenital anomalies with hypotonia and seizures type 1 or MCASH1. Affected infants have dysmorphic features, congenital macrocephaly, and renal and anorectal anomalies. Neurologic features include hypotonia, severe development delay and epilepsy manifesting in the neonatal period [Maydan et al., 2011]. Mutations in *PIGV*, *PIGO*, or *PGAP2* cause Mabry syndrome, also known as hyperphosphatasia with mental retardation or HPMRS [Mabry et al., 1970; Krawitz et al., 2010, 2013; Horn et al., 2011].

Author Manuscript Author Manuscript Author Manuscript Author Manuscript

Patients with mutations in multiple genes affecting GPI anchor biosynthesis share key phenotypic features with patients in the family reported here, including variably abnormal neurological development, intellectual impairment, and seizures. However, the in-frame *PIGA* deletion mutation described in this family produces a phenotype distinct from that observed with the *PIGA* truncation mutation reported by Johnston et al. [2012]. Individual IV-3 has normal red blood cell CD59 surface expression and is 15 years old at the time of this writing. The hematologic findings in this patient more closely resemble those previously reported in two families reported by Almeida et al. [2006, 2007] with a *PIGM* promoter mutation resulting in an inherited GPI deficiency, although the clinical phenotype is quite distinct. The reduction of FLAER staining and cell surface expression of CD24 on the granulocytes of the patient reported here indicates that the *PIGA* in-frame deletion mutation causes a reduction in PIGA activity in granulocytes. Since granulocytes were affected and red blood cells were unaffected, the p.Leu110del mutation PIGA activity reduction may be tissue or cell type dependent possibly due to *PIGA* transcription levels, the amount of PIGA activity required per cell type,or the role of the other PIG family cofactors in the initiating step of the GPI anchor biosynthesis pathway.

None of the reports of patients with germline mutations in genes coding for the PIG family enzymes have manifested systemic iron overload; however, patients with mutations in *PIGL* are reported to manifest an icthyosiform dermatitis. Since PIGA is the first enzyme in the GPI anchor biosynthesis pathway, iron overload may be specific to selective *PIGA* gene mutations. The family reported by Johnston et al. did not undergo iron studies (L. Biesecker, personal communication), and our data do not provide insights to the kinetics of iron load in the patients reported here. It is possible, given the similarities of neuroimaging features between the patients reported here and those reported by Johnston et al., [2012] that these represent phenotypic spectrums of the same disorder. We further examined the mother of patient IV-3 to see if there was laboratory or clinical evidence of iron overload, and did not detect any abnormalities. However, we can not exclude the possibility that some female carriers might in some cases manifest a mild phenotype. Although we considered the possibility that iron overload in the family reported here may be due to a separate mutation, analysis of the exome data of all known genes associated with hemochromatosis showed no likely causal variants. One plausible connection between the *PIGA* deletion and iron overload and hemochromatosis in the present family is the involvement of the GPI anchor protein hemojuvelin (HJV) in iron metabolism [Silvestri et al., 2007; Santos et al., 2012]. The HJV protein is found in skeletal muscle, heart and liver, and regulates hepcidin levels and therefore iron levels in various tissues, cell types, and serum [Zhang, 2011]. Mutations in *HJV* cause juvenile hemochromatosis (OMIM 602390). The p.Arg326X truncation mutation in particular lacks the N-terminus of the protein and the GPI anchor, and is not found on the cell surface of hepatocytes [Silvestri et al., 2007]. If the *PIGA* deletion reduces HJV cell surface expression, this could result in progressive systemic iron overload.

Several proteins involved in neurodevelopment are GPI-an-chored and their reduced expression has been proposed as a mechanism for the neurological disorders seen in families with other PIG family mutations. For instance, TAG1 and contactin are GPI anchor proteins in the central nervous system and have roles in neuronal development [Labasque and Faivre-

Author Manuscript Author Manuscript Author Manuscript Author Manuscript

Sarrailh, 2009]. The epidermal specific *Piga* null mouse indicated a role for PIGA in normal skin development, with affected mice demonstrating a Harlequin ichthyosis-like skin condition [Tarutani et al., 1997; Hara-Chikuma et al., 2004]. Ichthyosis was the initial manifestation of cutaneous abnormalities in our patients, although these lesions evolved over time to streaky, hyperpigmented linear and plaque like psoariform-like lesions. This mouse also demonstrated deficient processing of profilaggrin to filaggrin, a reaction accomplished by the GPI-anchored serine protease Prostasin (CAP/PRSS8) [Leyvraz et al., 2005]. Prostasin deficient epidermis results in a nearly complete loss of filaggrin and defective epidermal barrier function.

The affected individuals described here share some neurologic manifestations with the only previously reported family with a germline mutation in *PIGA*, including epilepsy and prominent cerebellar hypoplasia/atrophy. However, the family is unique in demonstrating systemic iron overload and unique cutaneous abnormalities and an absence of other congenital anomalies. This may suggest that the particular *PIGA* mutation reported here affects GPI-anchored proteins involved in iron homeostasis and skin and central nervous system development and function. The GPI-anchored proteins on the patient's granulocytes were reduced in amount, while those on the red blood cells and monocytes were at normal levels, providing evidence that the p.Leu110-del mutation *PIGA* activity reduction may be tissue or cell type-specific, possibly due to *PIGA* transcription levels, the amount of PIGA activity required per cell type, or the role of the other PIG family cofactors in the initiating step of the GPI anchor biosynthesis pathway. The FCC syndrome appears to be a selective and partial GPI deficiency (similar to the *PIGM* mutation syndrome) where only certain cell types appear affected by a reduction in GPI anchor protein cell surface expression. The delayed appearance of initial neurologic symptoms and prolonged survival of the patients with FCC syndrome, in contrast to the neonatal lethality reported by Johnston et al. [2012], indicates that the p.Leu110del *PIGA* mutation is less deleterious than the other reported *PIG* family mutations that eliminate all or most of GPI anchor protein expression, resulting in death in infancy. Since the mutant *PIGA* appears to retain some activity, potentially an increase in PIGA expression may help alleviate symptoms as has been reported anecdotally in patients deficient for PIGM, albeit likely less effective due to the nature of the *PIGM* mutation (promoter) versus the *PIGA* mutation (in-frame deletion). Further work is needed to understand which GPI-anchored proteins and cell types are affected most by the proposed reduced PIGA activity due to a single codon deletion mutation, and whether abnormal expression of HJV is implicated in causing systemic iron overload. Further, we need to understand the mechanism for progressive neurodegen-eration in the patients with FCC syndrome and if increasing PIGA levels (if possible) would be helpful to the patient, and at what point in the clinical course it might be effective. Identification of additional patients will ultimately help us to better understand the pathogenesis of this distinctive disorder.

ACKNOWLEDGMENTS

We are extremely grateful to the family for their participation in research studies over the course of many years. National Center for Research Resources Award Number UL1RR025764 to the University of Utah Clinical Center for Translational Science provided critical resources to help support this work. We also thank Drs. Jerry Kaplan, James Kushner, and Charles Parker for many helpful discussions and review of the data.

Author Manuscript Author Manuscript Author Manuscript Author Manuscript

Grant sponsor: National Institutes of Child Health and Disease; Grant sponsor: National Institutes of Neurologic Disease and Stroke; Grant sponsor: Muscular Dystrophy Association; Grant sponsor: Alternating Hemiplegia of Childhood Foundation.

REFERENCES

Almeida AM, Murakami Y, Layton DM, Hillmen P, Sellick GS, Maeda Y, Richards S, Patterson S, Kotsianidis I, Mollica L, Crawford DH, Baker A, Ferguson M, Roberts I, Houlston R, Kinoshita T, Karadimitris A. Hypomorphic promoter mutation in PIGM causes inherited glycosyl-phosphatidylinositol deficiency. Nat Med. 2006; 12:846–851. [PubMed: 16767100]

Almeida AM, Murakami Y, Baker A, Maeda Y, Roberts IA, Kinoshita T, Layton DM, Karadimitris A. Targeted therapy for inherited GPI deficiency. N Engl J Med. 2007; 356:1641–1647. [PubMed: 17442906]

Collardeau-Frachon S, Heissat S, Bouvier R, Fabre M, Baruteau J, Broue P, Cordier MP, Debray D, Debiec H, Ronco P, Guigonis V. A French retrospective multicentric study of neonatal hemochromatosis: Importance of autopsy and of auto-immune maternal manifestations. Pediatr Dev Pathol. 2012; 15:450–470. [PubMed: 22901025]

DePristo MA, Banks E, Poplin R, Garimella KV, Maguire JR, Hartl C, Philippakis AA, del Angel G, Rivas MA, Hanna M, McKenna A, Fennell TJ, Kernytsky AM, Sivachenko AY, Cibulskis K, Gabriel SB, Altshuler D, Daly MJ. A framework for variation discovery and genotyping using next-generation DNA sequencing data. Nat Genet. 2011; 43:491–498. [PubMed: 21478889]

González-Vioque E, Blázquez A, Fernández-Moreira D, Bornstein B, Bautista J, Arpa J, Navarro C, Campos Y, Fernández-Moreno MA, Garesse R, Arenas J, Martín MA. Association of novel POLG mutations and multiple mitochondrial DNA deletions with variable clinical phenotypes in a Spanish population. Arch Neurol. 2006; 63:107–111. [PubMed: 16401742]

Hara-Chikuma M, Takeda J, Tarutani M, Uchida Y, Holleran WM, Endo Y, Elias PM, Inoue S. Epidermal-specific defect of GPI anchor in PIG-A null mice results in har lequin ichthyosis-like features. J Invest Dermatol. 2004; 123:464–469. [PubMed: 15304084]

Horn D, Krawitz P, Mannhardt A, Korenke GC, Meinecke P. Hyperphosphatasia-mental retardation syndrome due to PIGV mutations: Expanded clinical spectrum. Am J Med Genet Part A. 2011; 155A:1917–1922. [PubMed: 21739589]

Jaeken J. Congenital disorders of glycosylation (CDG): It's (nearly) all in it! J Inherit Metab Dis. 2011; 34:853–858. [PubMed: 21384229]

Johnston JJ, Gropman AL, Sapp JC, Teer JK, Martin JM, Liu CF, Yuan X, Ye Z, Cheng L, Brodsky RA, Biesecker LG. The phenotype of a germline mutation in PIGA: The gene somatically mutated in paroxysmal nocturnal hemoglobinuria. Am J Hum Genet. 2012; 90:295–300. [PubMed: 22305531]

Keller P, Tremml G, Rosti V, Bessler M. X inactivation and somatic cell selection rescue female mice carrying a PIGA-null mutation. Proc Natl Acad Sci USA. 1999; 96:7479–7483. [PubMed: 10377440]

Kinoshita T, Ohishi K, Takeda J. GPI-anchor synthesis in mammalian cells: Genes, their products, and a deficiency. J Biochem. 1997; 122:251–257. [PubMed: 9378699]

Kinoshita T, Fujita M, Maeda Y. Biosynthesis, remodelling and functions of mammalian GPI-anchored proteins: Recent progress. J Biochem. 2008; 144:287–294. [PubMed: 18635593]

Krawitz PM, Schweiger MR, Rodelsperger C, Marcelis C, Kolsch U, Meisel C, Stephani F, Kinoshita T, Murakami Y, Bauer S, Isau M, Fischer A, Dahl A, Kerick M, Hecht J, Kohler S, Jager M, Grunhagen J, de Condor BJ, Doelken S, Brunner HG, Meinecke P, Passarge E, Thompson MD, Cole DE, Horn D, Roscioli T, Mundlos S, Robinson PN. Identity-by-descent filtering of exome sequence data identifies PIGV mutations in hyperphosphatasia mental retardation syndrome. Nat Genet. 2010; 42:827–829. [PubMed: 20802478]

Krawitz PM, Murakami Y, RieB A, Hietala M, Kruger U, Zhu N, Kinoshita T, Mundlos S, Hecht J, Robinson PN, Horn D. PGAP2 mutations, affecting the GPI-anchor-synthesis pathway, cause hyperphosphatasia with mental retardation syndrome. AJHG. 2013; 92:584–589.

Labasque M, Faivre-Sarrailh C. GPI-anchored proteins at the node of ranvier. FEBS Lett. 2009; 584:1787–1792. [PubMed: 19703450]

Author Manuscript Author Manuscript Author Manuscript Author Manuscript

Leyvraz C, Charles RP, Rubera I, Guitard M, Rotman S, Breiden B, Sandhoff K, Hummler E. The epidermal barrier function is dependent on the serine protease CAP1/PRSS8. J Cell Biol. 2005; 170:487–496. [PubMed: 16061697]

Luoma P, Melberg A, Rinne JO, Kaukonen JA, Nupponen NN, Chalmers RM, Oldfors A, Rautakorpi I, Peltonen L, Majamaa K, Somer H, Suomalainen A. Parkinsonism, premature menopause, and mitochondrial DNA polymerase gamma mutations: Clinical and molecular genetic study. Lancet. 2004; 364:875–882. [PubMed: 15351195]

Mabry CC, Bautista A, Kirk RF, Dubilier LD, Braunstein H, Koepke JA. Familial hyperphosphatase with mental retardation, seizures, and neurologic deficits. J Pediatr. 1970; 77:74–85. [PubMed: 5465362]

Maydan G, Noyman I, Har-Zahav A, Neriah ZB, Pasmanik-Chor M, Yeheskel A, Albin-Kaplanski A, Maya I, Magal N, Birk E, Simon AJ, Halevy A, Rechavi G, Shohat M, Straussberg R, Basel-Vanagaite L. Multiple congenital anomalies-hypotonia-seizures syndrome is caused by a mutation in PIGN. J Med Genet. 2011; 48:383–389. [PubMed: 21493957]

Ng BG, Hackmann K, Jones MA, Eroshkin AM, He P, Williams R, Bhide S, Cantagrel V, Gleeson JG, Paller AS, Schnur RE, Tinschert S, Zunich J, Hegde MR, Freeze HH. Mutations in the glycosylphosphatidylinositol gene PIGL cause CHIME syndrome. Am J Hum Genet. 2012; 90:685–688. [PubMed: 22444671]

Santos PC, Krieger JE, Pereira AC. Molecular diagnostic and pathogenesis of hereditary hemochromatosis. Int J Mol Sci. 2012; 13:1497–1511. [PubMed: 22408404]

Silvestri L, Pagani A, Fazi C, Gerardi G, Levi S, Arosio P, Camaschella C. Defective targeting of hemojuvelin to plasma membrane is a common pathogenetic mechanism in juvenile hemochromatosis. Blood. 2007; 109:4503–4510. [PubMed: 17264300]

Tarutani M, Itami S, Okabe M, Ikawa M, Tezuka T, Yoshikawa K, Kinoshita T, Takeda J. Tissue-specific knockout of the mouse PIG-A gene reveals important roles for GPI-anchored proteins in skin development. Proc Natl Acad Sci USA. 1997; 94:7400–7405. [PubMed: 9207103]

The 1000 genomes project consortium. A map of human genome variation from population-scale sequencing. Nature. 2010; 467:1061–1073. [PubMed: 20981092]

Ware RE, Rosse WF, Howard TA. Mutations within the PIGA gene in patients with paroxysmal nocturnal hemoglobinuria. Blood. 1994; 83:2418–2422. [PubMed: 8167330]

Zhang AS. Control of systemic iron homeostasis by the hemojuvelin-hepcidin axis. Adv Nutr. 2011; 1:38–45. [PubMed: 22043450]

Author Manuscript Author Manuscript Author Manuscript Author Manuscript

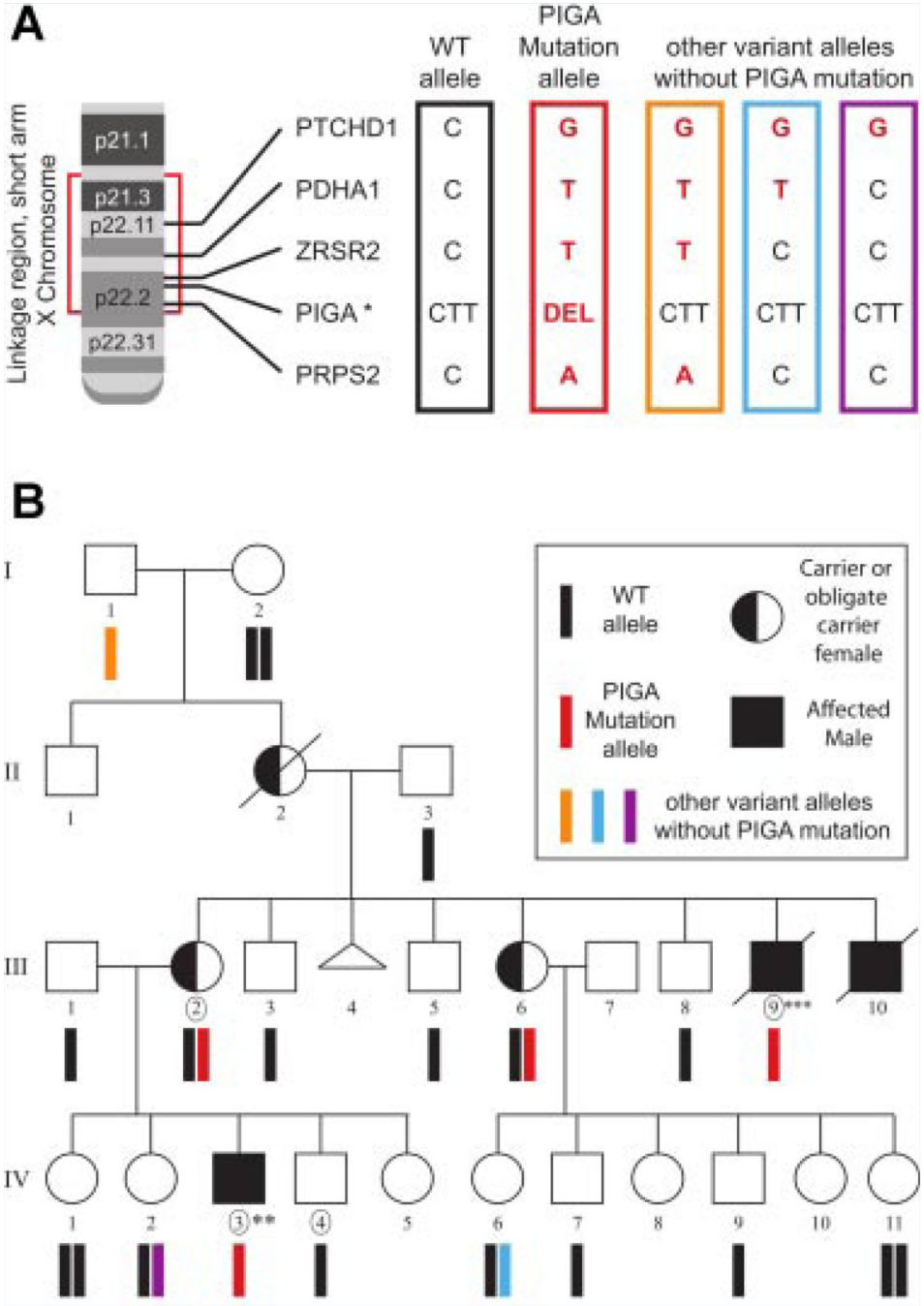

FIG. 1.

X chromosome alleles and pedigree. A: X chromosome is shown at the left, with the linkage area bracketed in red. The five rare variants followed by Sanger sequencing throughout the family are shown with the gene name and the location within the linkage region: *PTCHD1* (g.23410745C>G), *PDHA1* (g.19367346C>T), *ZRSR2* (g.15838411C>T), *PIGA* (g. 15342943-15342945delAAG), and *PRPS2* (g.12817576C>A). The *PIGA* gene (starred) is in the reverse orientation, so the wild type "CTT" codon for Leucine is deleted (DEL). The wild type allele (black) and the allele with the *PIGA* codon deletion (red) are shown, along

with three other allele variations (orange, blue, and purple). B: Family pedigree. Squares are male and circles are female. Filled squares indicate affected males, including the propositus IV-3 and his affected uncle III-9 . The half-filled circles are carrier females or obligate carriers. Exome-sequenced individuals are circled.

Author Manuscript Author Manuscript Author Manuscript Author Manuscript

Author Manuscript Author Manuscript Author Manuscript Author Manuscript

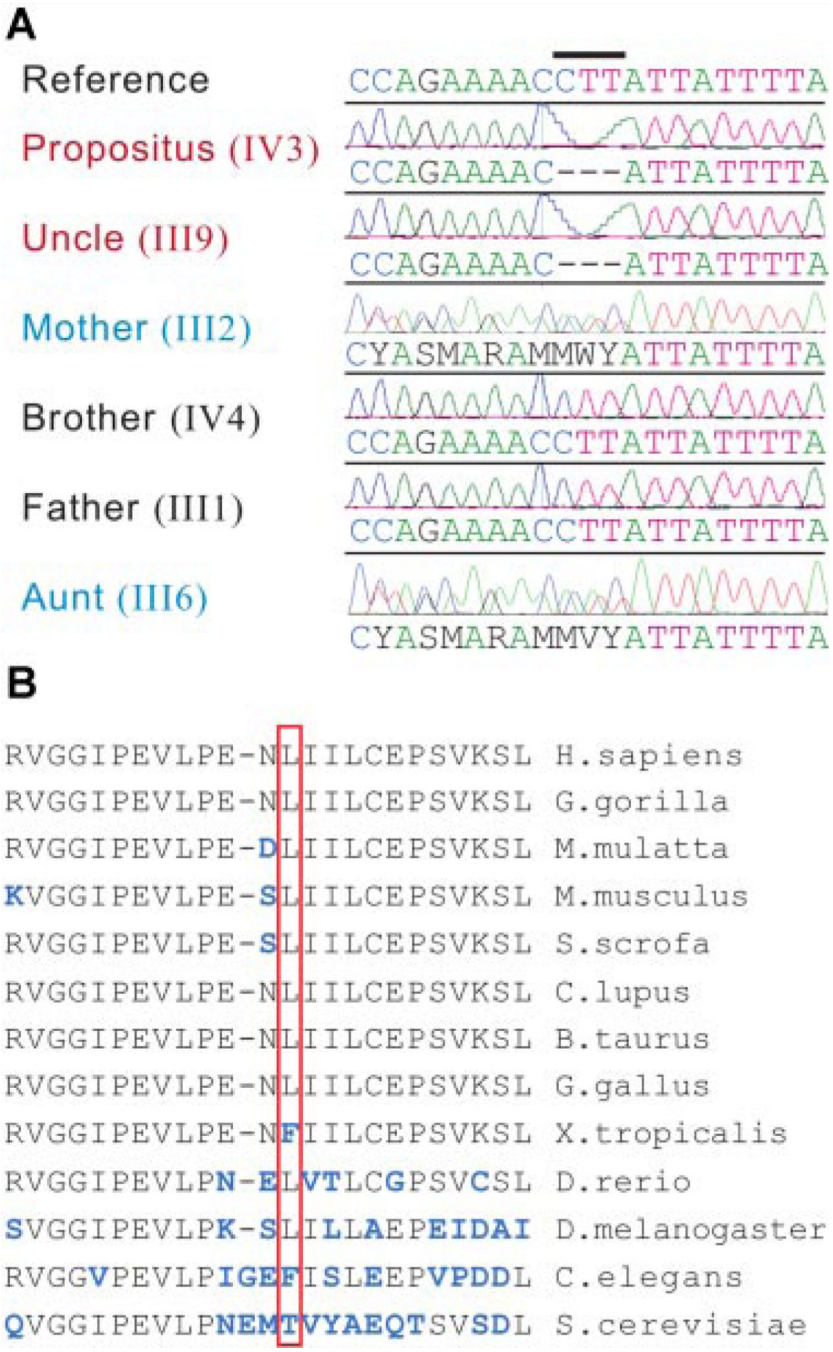

FIG. 2.

Sanger verification and multiple protein sequence alignment. A: All family members with available DNA samples were Sanger sequenced for the *PIGA* three base pair deletion variant position (marked with a bar, CTT). The example sequences shown are in the reverse direction, so the carriers (blue text label) have two sequences to the left of the mutation position due to being heterozygous for the three base pair deletion. The affected individuals have a red text label. The other family members not shown were all wild type at this

position. B: Multiple protein sequence alignment over the deleted amino acid of the *PIGA* gene (p.Leu110, boxed in red) is shown from human to fish and fruit fly sequences.

Author Manuscript Author Manuscript Author Manuscript Author Manuscript

Author Manuscript Author Manuscript Author Manuscript Author Manuscript

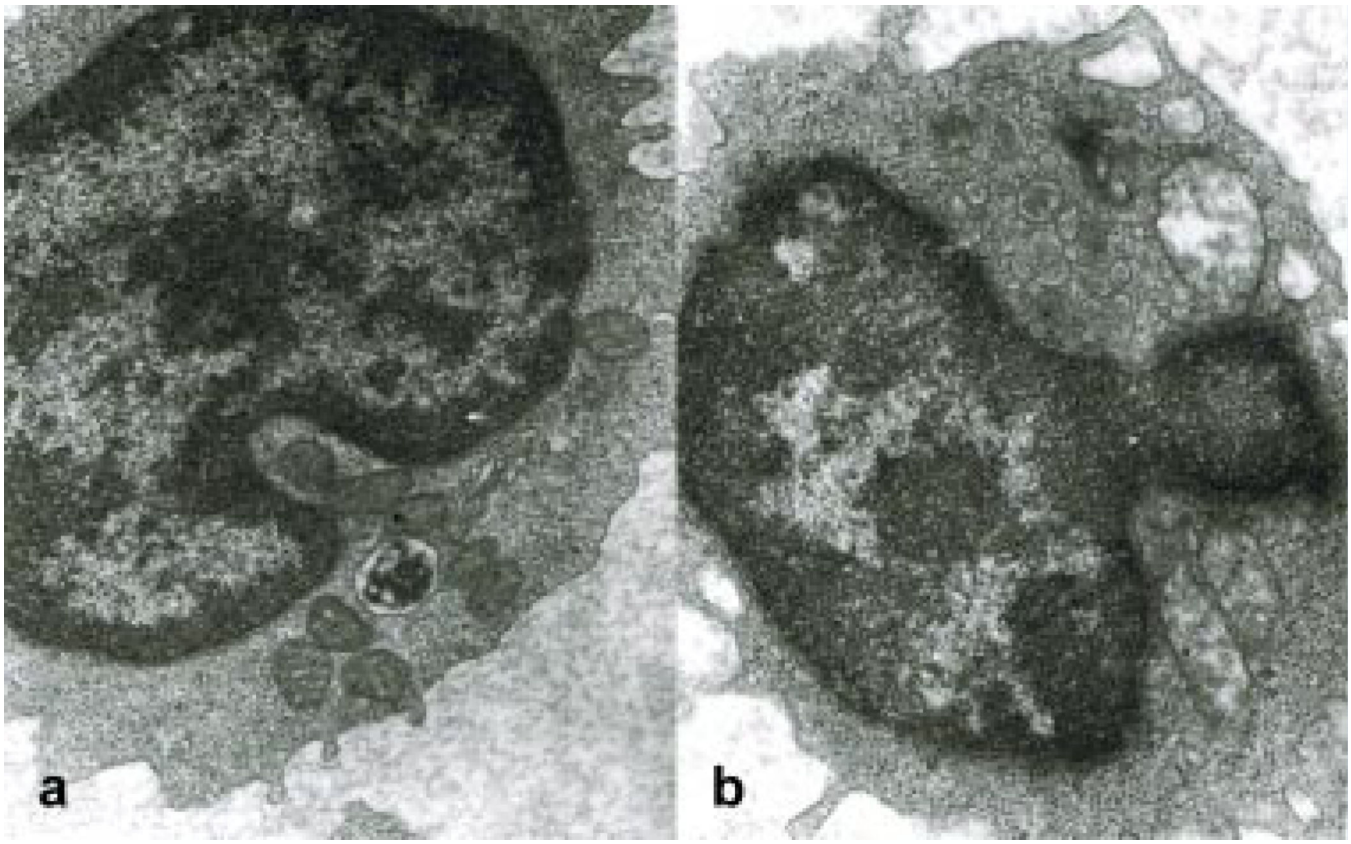

FIG. 3.

Electron microscopic leukocyte studies demonstrated lymphocytes with small myelin figures and clusters of vacuoles with electron dense tubules; a siderosome is evident in 6a as indicated by arrowhead.

Author Manuscript Author Manuscript Author Manuscript Author Manuscript

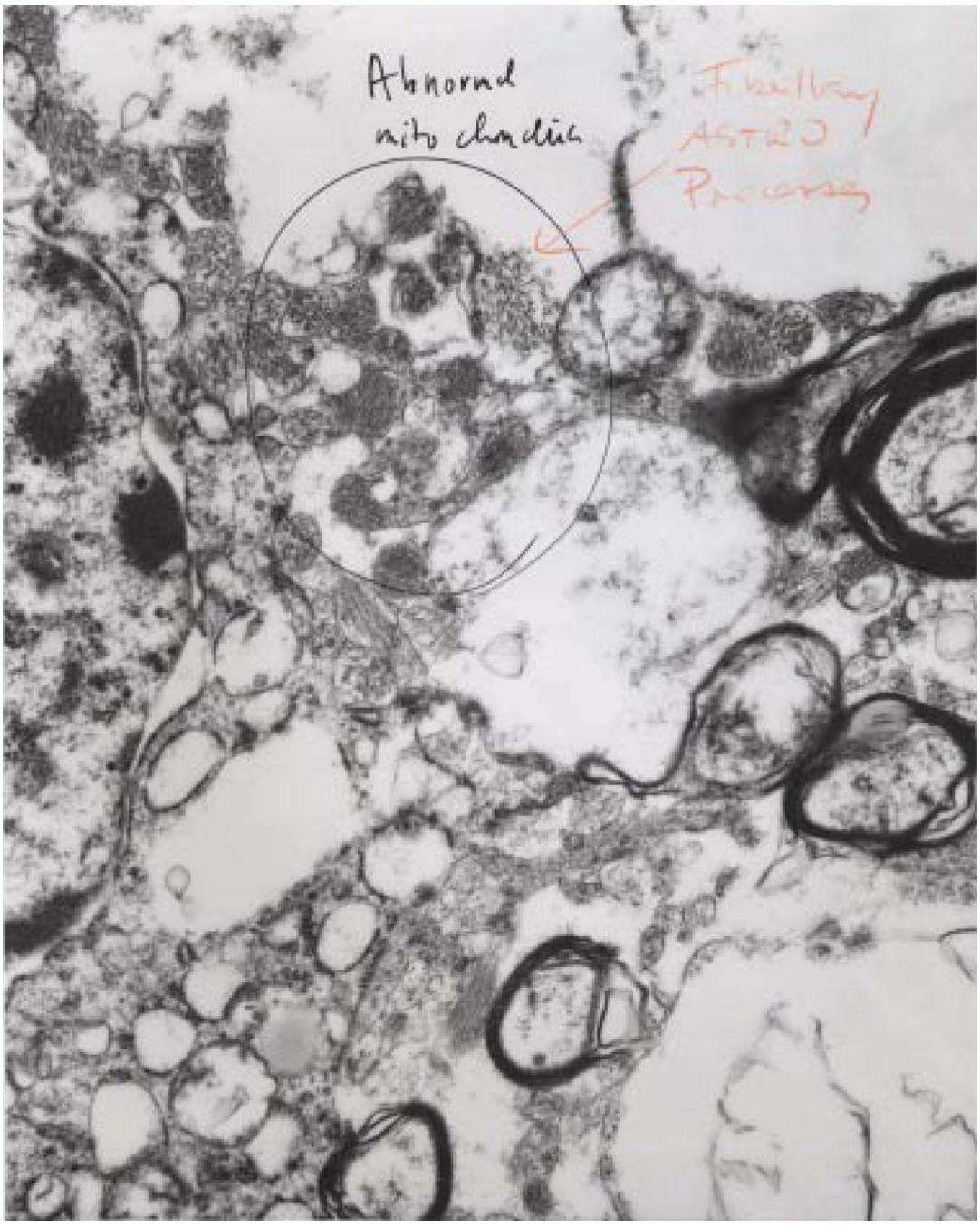

FIG. 4.

Electron micrographs of brain from a frontal lobe biopsy in III-9 at age 5 years demonstrated abnormal appearing mitochondria and fibrillary astrocytic processes.

Author Manuscript Author Manuscript Author Manuscript Author Manuscript

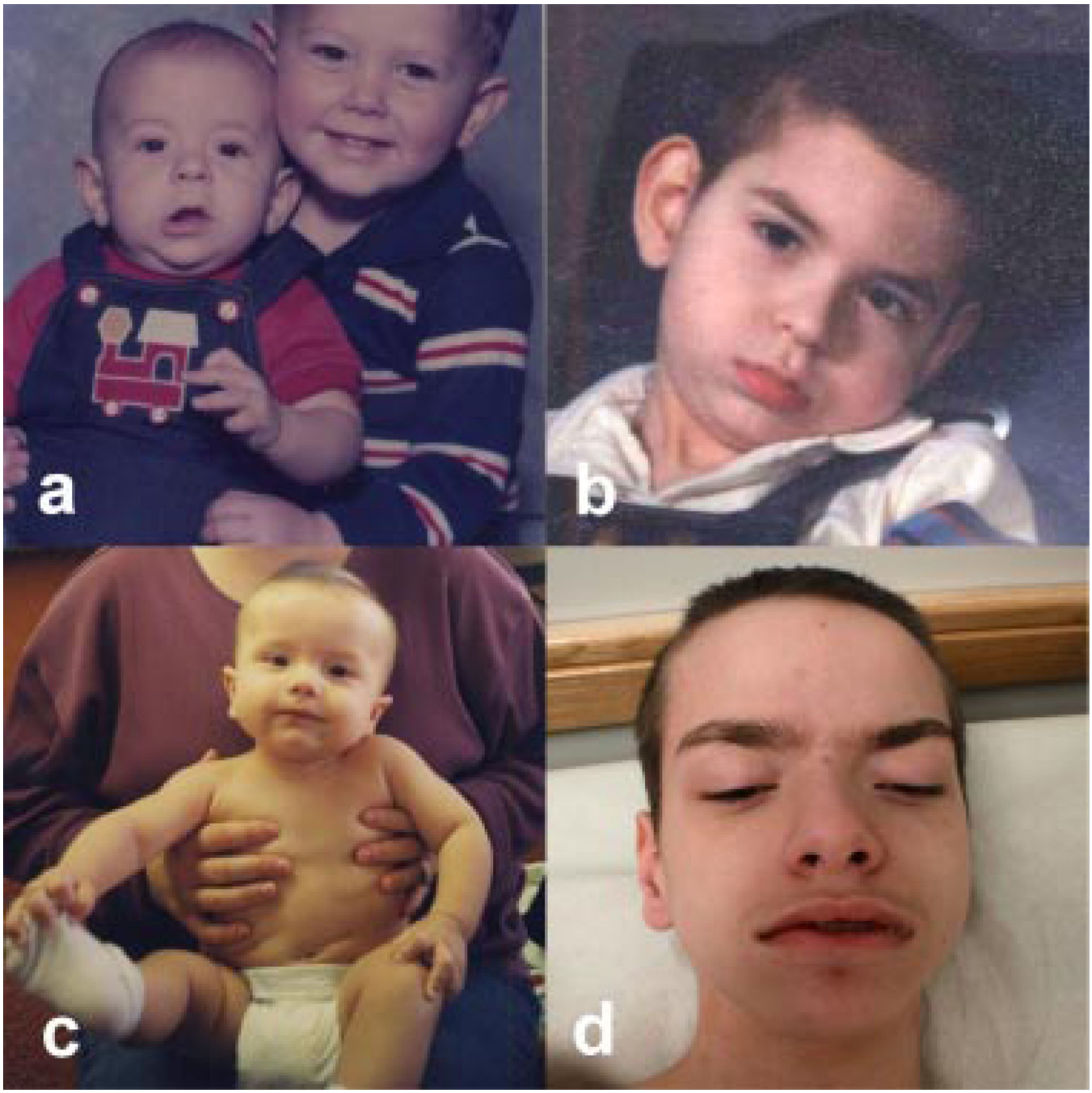

FIG. 5.

Photos of affected males. (a) Individual III-10 at age 6 months, and (b) at age 5 years. (c) Individual IV-3 at 6 months and (d) vegetative, at age 14 years.

Author Manuscript Author Manuscript Author Manuscript Author Manuscript

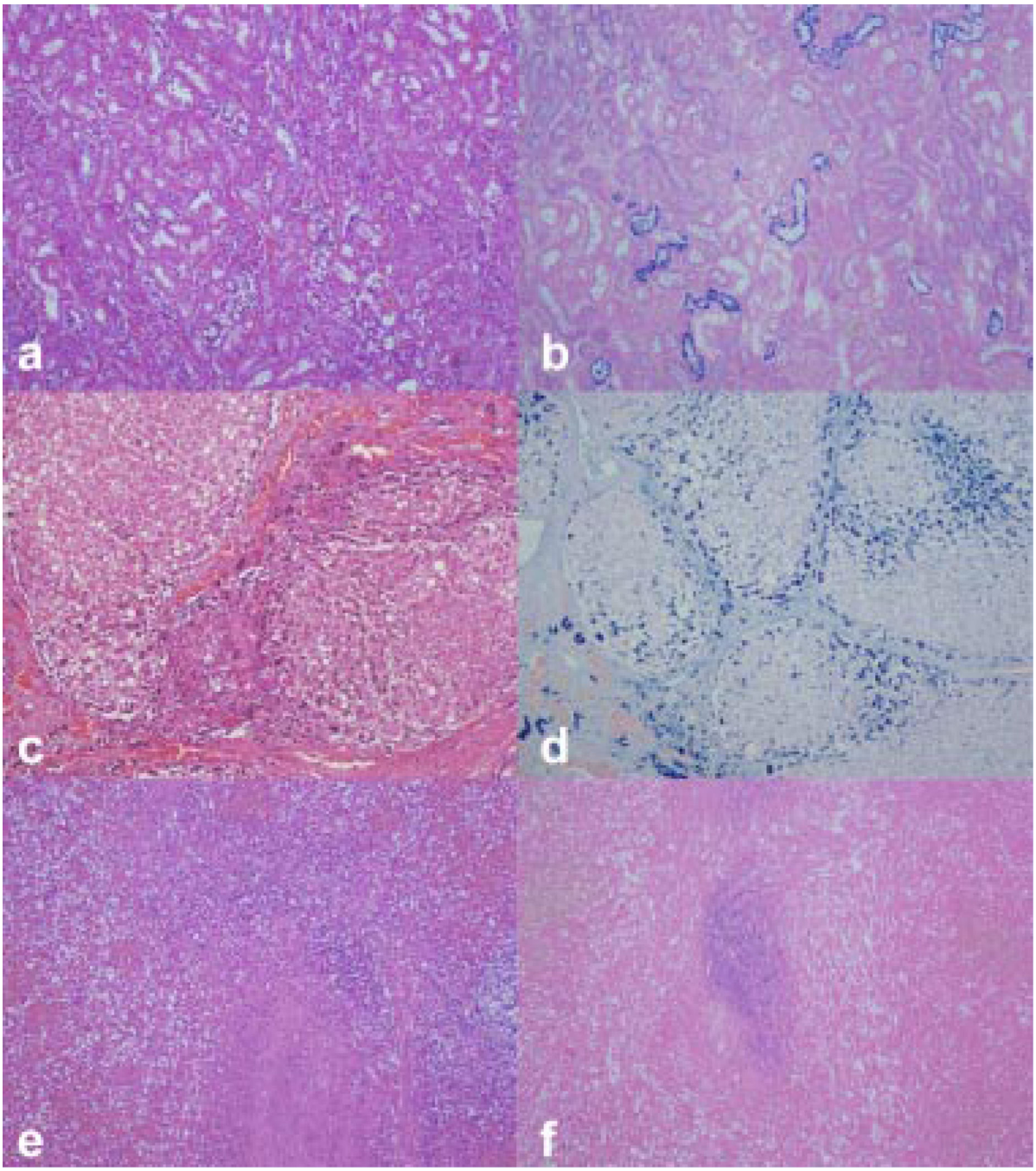

FIG. 6.

Histological sections from kidney, liver, and spleen from autopsy (III-9). a: Brown pigments in renal tubules (H&E×100). b: The pigments were positive for iron-Prussian blue stain (×100). c: Cirrhotic nodules with fatty change (H&E, ×200). d: Marked accumulation of hemosiderin in hepatocytes was present (Iron-Prussian blue stain, × 200). e: No grossly evident pigment deposition in spleen (H&E, × 100). f: Patchy iron deposition in spleen (Iron-Prussian blue stain, × 100).

Author Manuscript Author Manuscript Author Manuscript Author Manuscript

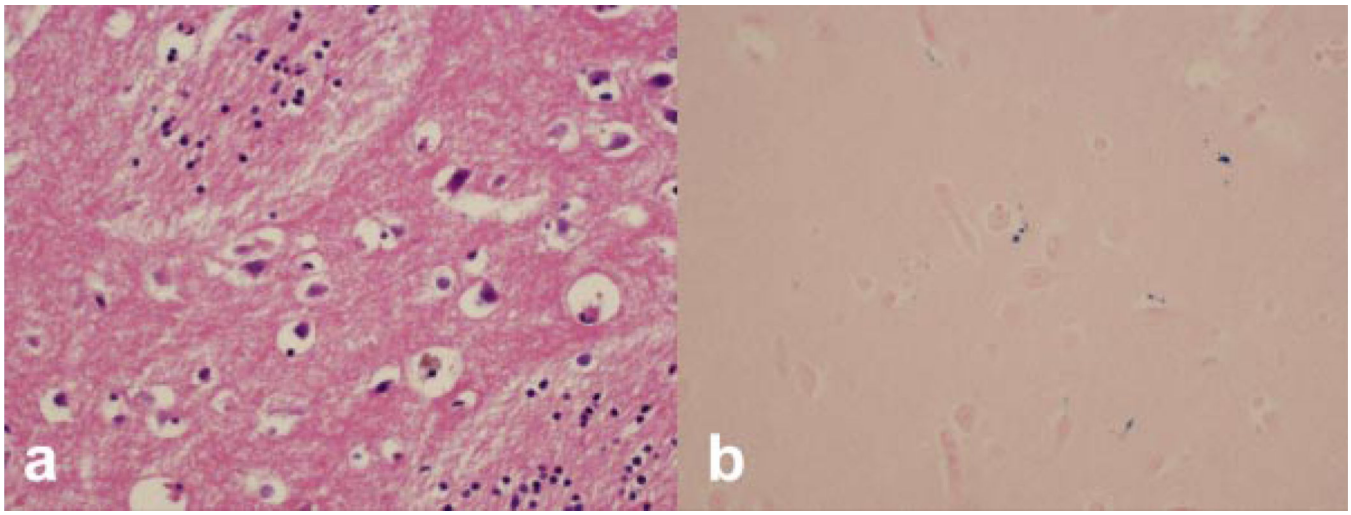

FIG. 7.

Scant iron deposition in brain from autopsy (III-9)—Basal Ganglia. a: Rare sections of basal ganglia showed brown pigments in neurons (H&E × 400). b: Iron-Prussian blue stain demonstrated that the pigments were positive for iron staining (×400).

Author Manuscript
Author Manuscript
Author Manuscript
Author Manuscript

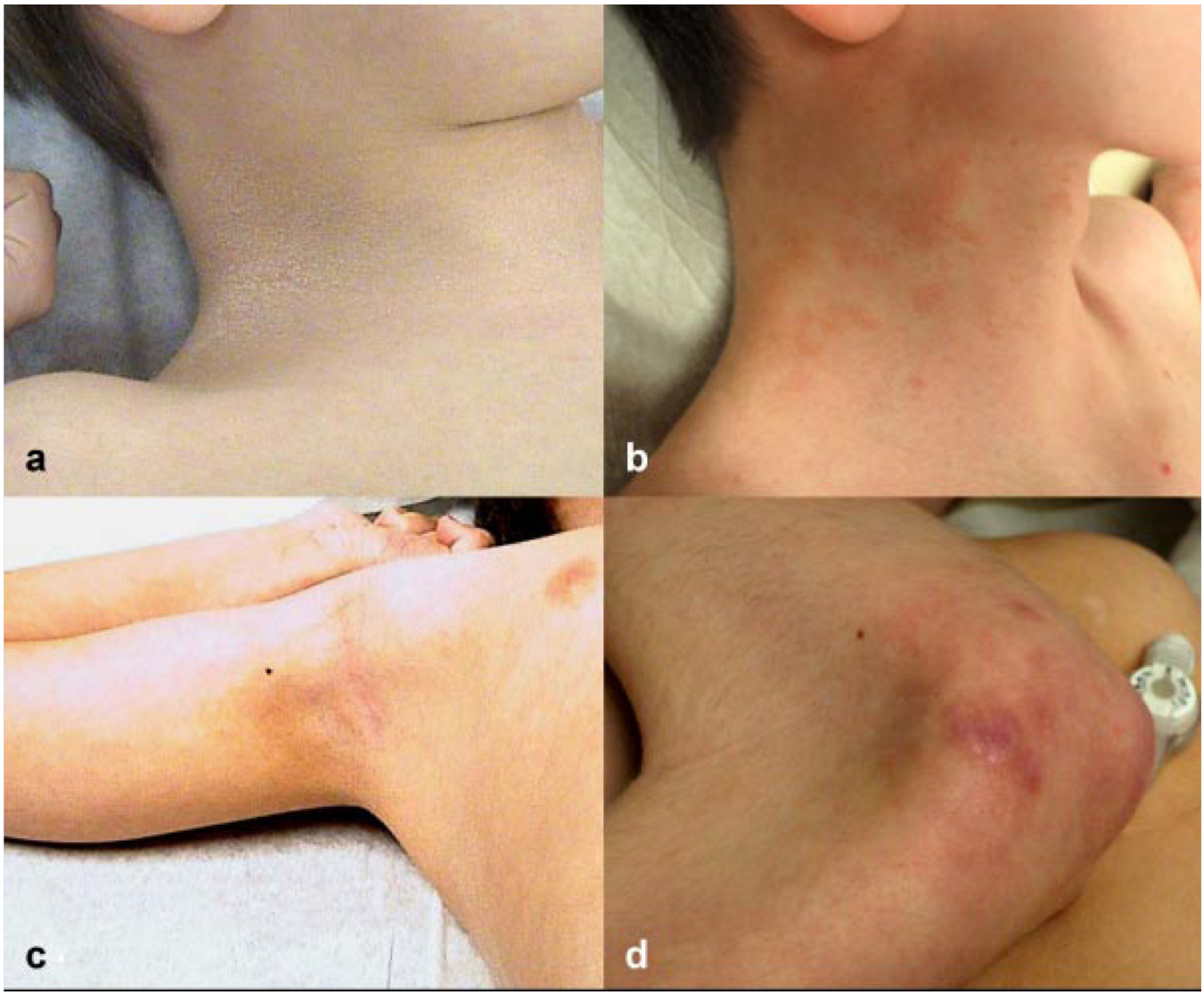

FIG. 8.

Evolution of skin lesions with age, individual IV-3. a: Ichthyosis, age 5½ years. b: Yellowish brown plaque-like neck lesions, age 14 years. c: Streaky axillary and trunk hyperpigmentation, age 5½ years. d: Elbow lesions, age 14 years.

Author Manuscript Author Manuscript Author Manuscript Author Manuscript

FIG. 9.

Cutaneous and oral abnormalities, individual IV-3. (a) Epidermal microabscesses (b) microdontia, with widely spaced pointed teeth and gingival overgrowth are representative of those in all three affected males. c: Foot deformity and skin lesions, age 14 years.

Author Manuscript Author Manuscript Author Manuscript Author Manuscript

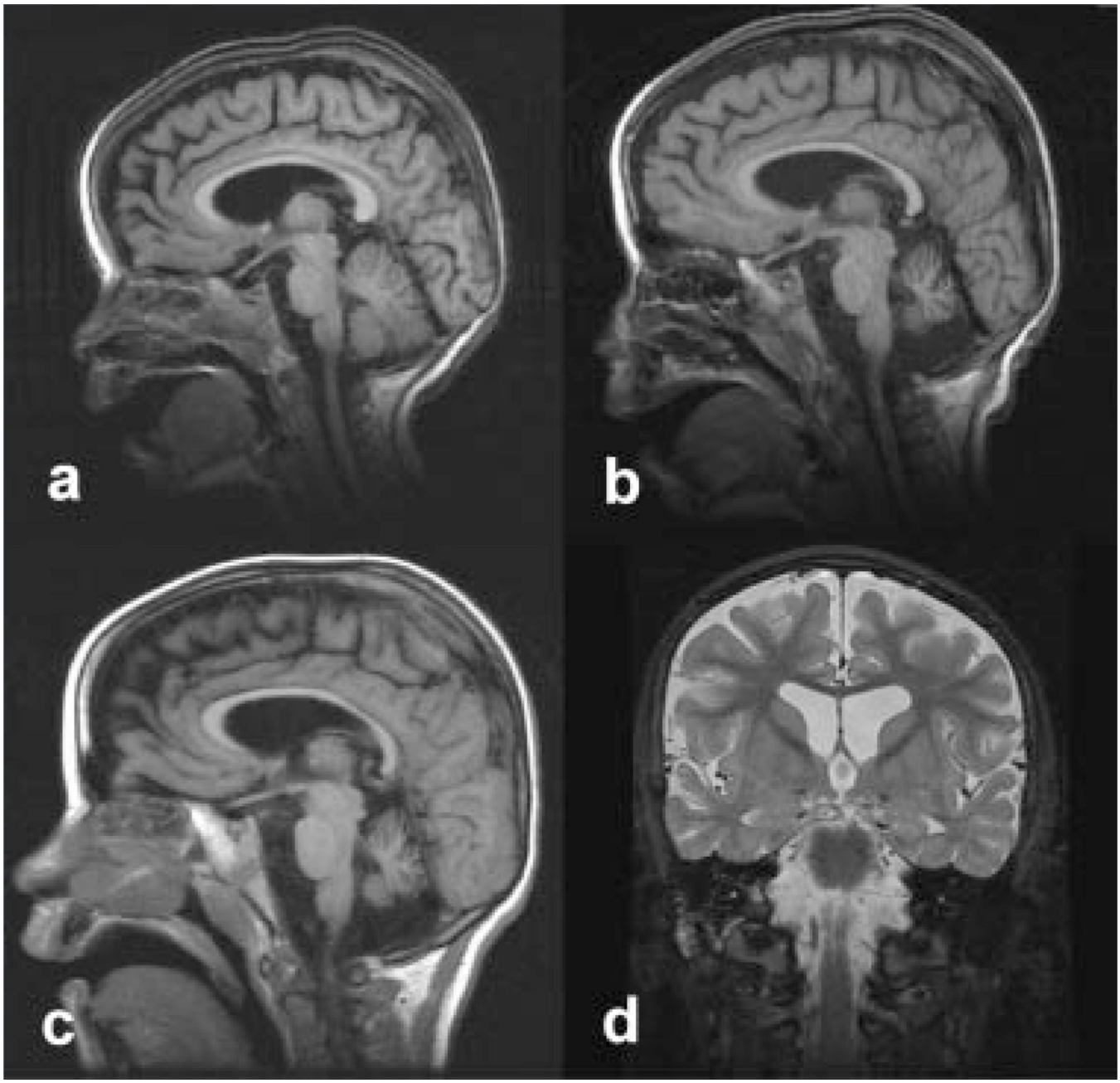

FIG. 10.

Neuroimaging features. Serial MRI images in individual IV-3 demonstrated progressive cerebellar and to a lesser extent cerebral atrophy and white matter loss at ages (a) 8 months, (b) 3½ years, and (c) 5½ years. d: Stir images performed at age 5½ years failed to demonstrate excess brain iron deposition.

Author Manuscript Author Manuscript Author Manuscript Author Manuscript

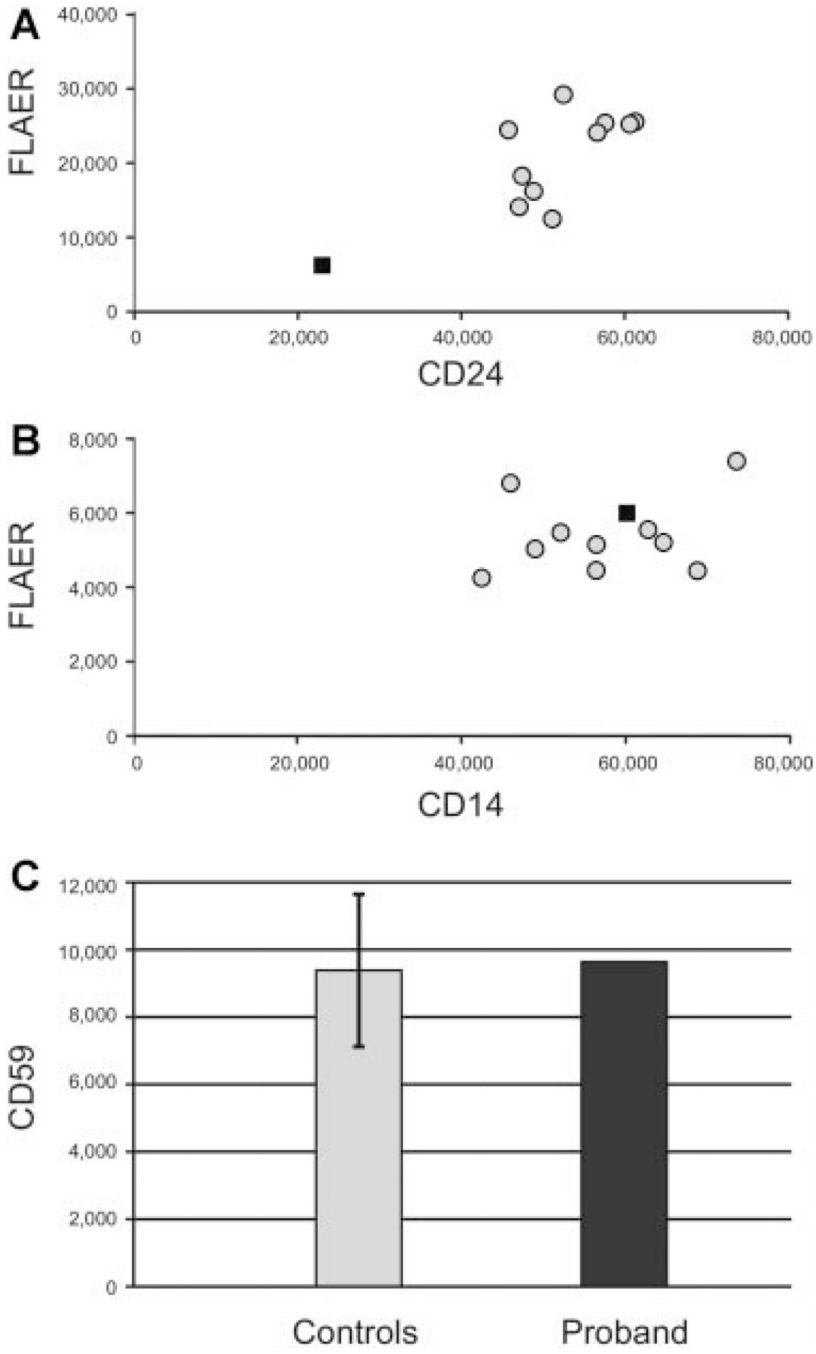

FIG. 11.

Experiments showing GPI-anchored protein levels in blood cells. A and B: Cell surface expression of GPI-anchored proteins was assayed by flow cytometry. FLAER is a stain for GPI expression. The sample from IV-3 is the black square, and the 10 normal controls are the gray circles. A: FLAER and CD24 were tested for the granulocytes. B: FLAER and CD14 were tested for the monocytes. C: CD59 cell surface expression on the red blood cells.

Author Manuscript Author Manuscript Author Manuscript Author Manuscript

The gray bar is the average for ten controls (with SD marked), and the black bar is IV-3's data.